

Tenth-Order QED Lepton Anomalous Magnetic Moment — Eighth-Order Vertices Containing a Second-Order Vacuum Polarization

Tatsumi Aoyama,^{1,2} Masashi Hayakawa,^{3,2} Toichiro Kinoshita,^{4,2} and Makiko Nio²

¹*Kobayashi-Maskawa Institute for the Origin of Particles and the Universe (KMI),
Nagoya University, Nagoya 464-8602, Japan*

²*Nishina Center, RIKEN, Wako 351-0198, Japan*

³*Department of Physics, Nagoya University, Nagoya 464-8602, Japan*

⁴*Laboratory for Elementary-Particle Physics,
Cornell University, Ithaca, New York 14853, USA*

(Dated: November 27, 2024)

Abstract

This paper reports the evaluation of the tenth-order QED contribution to the lepton $g-2$ from the gauge-invariant set of 2072 Feynman diagrams, called Set IV, which are obtained by inserting a second-order lepton vacuum-polarization loop into 518 eighth-order vertex diagrams of four-photon exchange type. The numerical evaluation is carried out by the adaptive-iterative Monte-Carlo integration routine VEGAS using the FORTRAN codes written by the automatic code-generating algorithm GENCODEN. Some of the numerical results are confirmed by comparison with the values of corresponding integrals that have been obtained previously by a different method. The result for the mass-independent contribution of the Set IV to the electron $g-2$ is $-7.7296 (48)(\alpha/\pi)^5$. There is also a small mass-dependent contribution to the electron $g-2$ due to the muon loop: $-0.01136 (7)(\alpha/\pi)^5$. The contribution of the tau-lepton loop is $-0.0000937 (104) (\alpha/\pi)^5$. The sum of all these contributions to the electron $g-2$ is $-7.7407 (49)(\alpha/\pi)^5$. The same set of diagrams enables us to evaluate the contributions to the muon $g-2$ from the electron loop, muon loop, and tau-lepton loop. They add up to $-46.95 (17)(\alpha/\pi)^5$.

PACS numbers:

I. INTRODUCTION

The anomalous magnetic moment $g-2$ of the electron has played the central role in testing the validity of quantum electrodynamics (QED) as well as the standard model. On the experimental side, the latest measurement of $a_e \equiv (g-2)/2$ by the Harvard group has reached the precision of 0.24×10^{-9} [1, 2]:

$$a_e(\text{HV08}) = 1\,159\,652\,180.73 (0.28) \times 10^{-12} \quad [0.24\text{ppb}]. \quad (1)$$

The theoretical prediction thus far consists of QED corrections of up to the eighth order [3–5], direct evaluation of hadronic corrections [6–8] [9–12] and electroweak corrections scaled down from their contributions to the muon $g-2$ [13–15]. To compare the theory with the measurement (1), we also need the value of the fine structure constant α determined by a method independent of $g-2$. The best value of such an α available at present is one obtained from the measurement of h/m_{Rb} , the ratio of the Planck constant and the mass of Rb atom, combined with the very precisely known Rydberg constant and m_{Rb}/m_e : [16]

$$\alpha^{-1}(\text{Rb10}) = 137.035\,999\,037 (91) \quad [0.66\text{ppb}]. \quad (2)$$

With this α the theoretical prediction of a_e becomes

$$a_e(\text{theory}) = 1\,159\,652\,181.13 (0.11)(0.37)(0.02)(0.77) \times 10^{-12}, \quad (3)$$

where the first, second, third, and fourth uncertainties come from the calculated eighth-order QED term [5], a crude tenth-order estimate [17], the hadronic and electroweak contributions, and the fine structure constant (2), respectively. The theory (3) is in good agreement with the experiment (1):

$$a_e(\text{HV08}) - a_e(\text{theory}) = -0.40 (0.88) \times 10^{-12}, \quad (4)$$

proving that QED (standard model) is in good shape even at this very high precision.

An alternative and more sensitive test of QED is to calculate α from the experiment and theory of $g-2$, both of which have very high precision, and compare it with $\alpha^{-1}(\text{Rb10})$. The experiment and theory of the electron $g-2$ leads

$$\alpha^{-1}(a_e08) = 137.035\,999\,085 (12)(37)(2)(33) \quad [0.37\text{ppb}], \quad (5)$$

where the first, second, third, and fourth uncertainties come from the eighth-order QED term, the tenth-order estimate, the hadronic and electroweak contributions, and the measurement of a_e (HV08), respectively.

Although the uncertainty of $\alpha^{-1}(a_e08)$ in (5) is almost a factor 2 smaller than that of $\alpha^{-1}(\text{Rb10})$, it is not a firm factor since it depends on the estimate of the tenth-order term, which is only a crude guess [17]. For a more stringent test of QED, it is obviously necessary to evaluate the actual value of the tenth-order term. To meet this challenge we launched several years ago a systematic program to evaluate the complete tenth-order term [18–20].

The tenth-order QED contribution to the anomalous magnetic moment of an electron can be written as

$$a_e^{(10)} = \left(\frac{\alpha}{\pi}\right)^5 \left[A_1^{(10)} + A_2^{(10)}(m_e/m_\mu) + A_2^{(10)}(m_e/m_\tau) + A_3^{(10)}(m_e/m_\mu, m_e/m_\tau) \right], \quad (6)$$

where the electron-muon mass ratio m_e/m_μ is $4.836\,331\,66(12) \times 10^{-3}$ and the electron-tau mass ratio m_e/m_τ is $2.875\,64(47) \times 10^{-4}$ [17]. In the rest of this article the factor $(\alpha/\pi)^5$ will be suppressed for simplicity.

The contribution to the mass-independent term $A_1^{(10)}$ can be classified into six gauge-invariant sets, further divided into 32 gauge-invariant subsets depending on the nature of closed lepton loop subdiagrams. Thus far, the numerical results of 29 gauge-invariant subsets, which consist of 3856 vertex diagrams, have been published [3, 21–27]. Five of these 29 subsets were also known analytically [28, 29]. They are in good agreement with our calculations.

In this paper we report the result of evaluation of $A_1^{(10)}$ from the set, called Set IV, which consists of 2072 Feynman diagrams. Sec. II outlines our formulation of Feynman-parametric integrals of Set IV. Sec. III presents the residual renormalization formula, which summarizes the result of derivation described in detail in Appendix A. Numerical results for several cases of mass dependence are described in Secs. IV, V, and VI. Sec. VII discusses the results obtained in this paper.

II. CONSTRUCTION OF FEYNMAN-PARAMETRIC INTEGRALS

All 2072 diagrams of Set IV can be derived from the 518 eighth-order diagrams of four-photon-exchange type [30], called Group V, by inserting a second-order vacuum-polarization

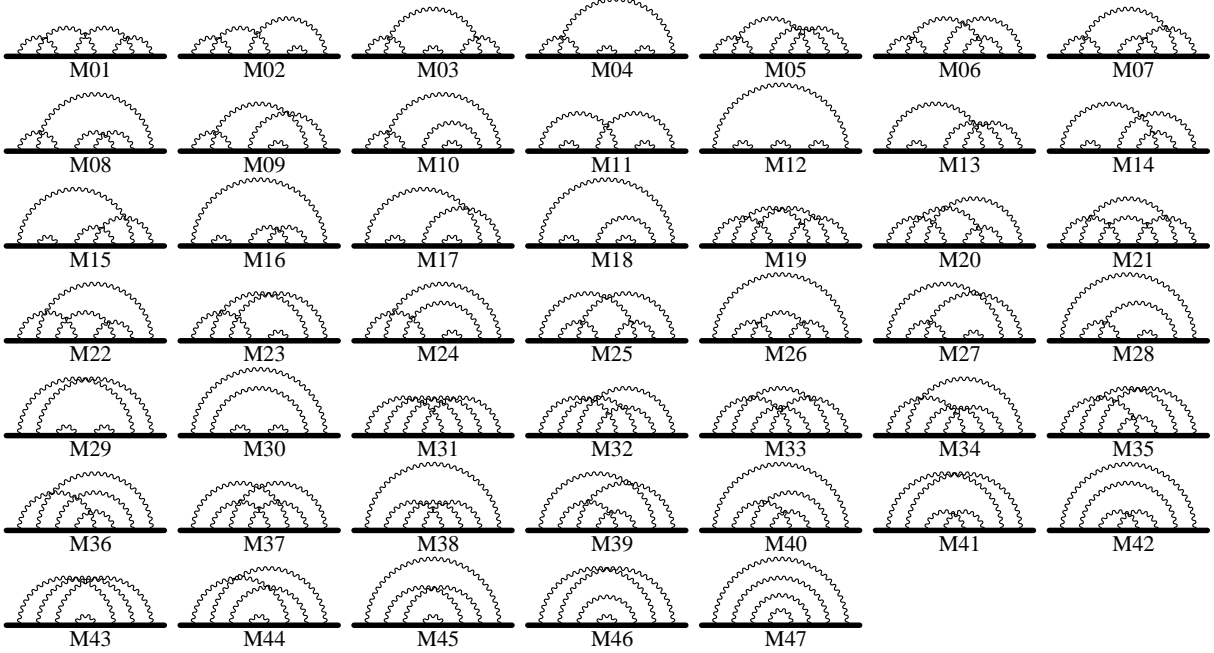


FIG. 1: The eighth-order Group V diagrams. The solid line represents the electron propagating in a weak constant magnetic field.

loop in the photon lines of Group V diagrams in all possible ways. In practice, we have therefore to deal with only 518 diagrams. This can be reduced further to the 47 self-energy-like diagrams of Fig. 1 as follows.

Let Λ^ν be the sum of 7 vertex diagrams that are obtained from any self-energy-like diagram $\Sigma(p)$ of Fig. 1 by inserting a magnetic vertex γ^ν in all possible ways. The set of these vertex diagrams, taking account of doubling due to time-reversal, represents the original 518 vertex diagrams. The next step is to rewrite this Λ^ν as

$$\Lambda^\nu(p, q) \simeq -q^\mu \left[\frac{\partial \Lambda_\mu(p, q)}{\partial q_\nu} \right]_{q=0} - \frac{\partial \Sigma(p)}{\partial p_\nu} \quad (7)$$

for small q , with the help of the Ward-Takahashi(WT) identity, where $p - q/2$ and $p + q/2$ are the 4-momenta of incoming and outgoing lepton lines and $(p - q/2)^2 = (p + q/2)^2 = m^2$. The $g-2$ term is projected out from the right-hand side of Eq. (7).

The properties of the Feynman-parametric integrals corresponding to the diagrams of Fig. 1 have been studied and described in detail in Ref. [5]. Each diagram \mathcal{G} of Fig. 1 is represented by a momentum integral using the Feynman-Dyson rule. Introducing Feynman parameters z_1, z_2, \dots, z_7 for the electron propagators and z_a, z_b, z_c, z_d for the photon propagators, we carry out the momentum integration analytically using a home-made program

written in FORM [31], which gives an integral of the form

$$M_{\mathcal{G}} = \left(\frac{-1}{4}\right)^4 3! \int (dz)_{\mathcal{G}} \left[\frac{1}{3} \left(\frac{E_0 + C_0}{U^2 V^3} + \frac{E_1 + C_1}{U^3 V^2} + \dots \right) + \left(\frac{N_0 + Z_0}{U^2 V^4} + \frac{N_1 + Z_1}{U^3 V^3} + \dots \right) \right], \quad (8)$$

where E_n, C_n, N_n and Z_n are functions of Feynman parameters. The subscript n of E_n , etc., indicates that it is the n contraction terms of diagonalized loop momenta and proportional to the product of n factors of B_{ij} 's. The ‘‘symbolic’’ building blocks A_i, B_{ij}, C_{ij} , for $i, j = 1, 2, \dots, 7$ are also functions of Feynman parameters. U is the Jacobian of transformation from the momentum space variables to Feynman parameters. V is obtained by combining denominators of all propagators into one with the help of Feynman parameters. It has a form common to all diagrams of Fig. 1:

$$V = \sum_{i=1}^7 z_i (1 - A_i) m_i^2 + \sum_{k=a}^d z_k \lambda_k^2, \quad (9)$$

where m_i and λ_k are the rest masses of electron i and photon k , respectively. A_i is the *scalar current* defined by

$$A_i = \delta_{ij} - \frac{1}{U} \sum_{j=1}^7 z_j B_{ij}, \quad (10)$$

and

$$(dz)_{\mathcal{G}} = \prod_{i \in \mathcal{G}} dz_i \delta(1 - \sum_{i \in \mathcal{G}} z_i). \quad (11)$$

See, for example, Ref. [32] for definitions of B_{ij} and C_{ij} . The form of A_i as a function of Feynman parameters depends on the structure of individual diagram. However, as is shown in Eq. (9), the expression of V in terms of A_i is identical for all diagrams of Fig. 1. Individual diagram of Fig. 1 will be denoted as $M_{\mathcal{G}}$ and their assembly will be collectively denoted as M_8 .

We have developed two independent sets of numerical programs of $M_{\mathcal{G}}$ based on the WT-summed amplitudes. The first formulation was developed in 1970's and given in Ref. [33]. The second formulation used the automation code `GENCODEN` [19, 20]. The unrenormalized amplitudes and the UV-subtraction terms are the same, but the IR-subtractions are slightly different in two formulations. The detail of UV- and IR-subtraction terms in the second formulation is briefly described in Sec. III. After taking account of the difference in two formulations, the equivalence of two formulations is established [20]. Once we have the correct programs of the eighth-order Group V diagrams, the insertion of a vacuum-polarization

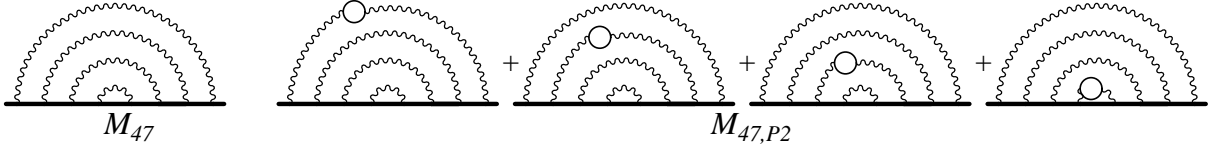


FIG. 2: The eighth-order diagram M_{47} of Group V and the tenth-order diagram $M_{47,P2}$ of Set IV. The diagram $M_{47,P2}$ represents the sum of diagrams obtained by inserting a second-order vacuum-polarization loop into each of four photon lines of the eighth-order diagram M_{47} .

loop is an easy task to carry out. Fig. 2 shows a typical self-energy-like diagram of the tenth-order Set IV.

As is well-known, the insertion of a vacuum-polarization loop in an internal photon line can be expressed as a superposition of massive vector particle propagators. In other words all we have to do is to replace the mass square λ^2 of one of the photons in Eq. (9) by $p(t)$:

$$\lambda^2 \longrightarrow p(t) \equiv \frac{4m_{vp}^2}{1-t^2}, \quad (12)$$

where m_{vp} is the mass of the fermion forming the vacuum-polarization loop, to multiply the resulting eighth-order integral with the spectral function

$$\rho_2(t) = \frac{t^2}{1-t^2} \left(1 - \frac{1}{3}t^2 \right), \quad (13)$$

and to integrate over the interval $0 \leq t < 1$.

This is easy to implement in the second formulation [19, 20] since the function V is unambiguously identifiable. Unfortunately, in the first formulation [33], it is difficult to implement this procedure for some diagrams because the “*denominator function V*” was used to replace parts of numerators in order to reduce the size of integrands and accelerate the computing speed. For this reason, it is difficult to apply Eqs. (12) and (13) to these integrals. Thus, direct comparison of two methods is feasible only for those of Set IV diagrams in which the function V can be clearly distinguished from other terms of the numerator. We therefore report here only the results of the second formulation. Since the equivalence of two methods has been well established [5], this does not diminish the reliability of our numerical results.

III. RESIDUAL RENORMALIZATION

In our approach based on numerical integration the integrals of individual diagrams must be made convergent before they are integrated numerically. This is achieved in the following manner.

Suppose the integral M_G has a UV divergence arising from a subdiagram \mathcal{S} . Then we construct another integral $K_{\mathcal{S}}M_G$ by applying a K -operation, which identifies and extracts the UV divergent part of M_G by a simple power counting rule. This integral has the following properties:

- It has the same domain of integration and the same UV divergence as M_G . Thus it subtracts the UV divergence of the latter *point-by-point* in the domain of integration.
- If \mathcal{S} is a vertex diagram, K -operation $\mathbb{K}_{\mathcal{S}}$ on M_G factorizes exactly into the product of lower-order quantities as

$$\mathbb{K}_{\mathcal{S}}M_G = L_{\mathcal{S}}^{\text{UV}}M_{G/\mathcal{S}}. \quad (14)$$

If \mathcal{S} is a self-energy diagram, K -operation $\mathbb{K}_{\mathcal{S}}$ on M_G turns exactly into the sum of two terms of the form

$$\mathbb{K}_{\mathcal{S}}M_G = \delta m_{\mathcal{S}}^{\text{UV}}M_{G/\mathcal{S}(i^*)} + B_{\mathcal{S}}^{\text{UV}}M_{G/\mathcal{S}(i')}. \quad (15)$$

Here $L_{\mathcal{S}}^{\text{UV}}$, $B_{\mathcal{S}}^{\text{UV}}$, and $\delta m_{\mathcal{S}}^{\text{UV}}$ are UV-divergent parts of the renormalization constants $L_{\mathcal{S}}$, $B_{\mathcal{S}}$, and $\delta m_{\mathcal{S}}$. $M_{G/\mathcal{S}}$ is the magnetic moment corresponding to the diagram \mathcal{G}/\mathcal{S} obtained by shrinking the subdiagram \mathcal{S} of \mathcal{G} to a point. See Ref. [32] for further details.

An IR divergence of M_G arises from a subdiagram \mathcal{T} that is the reduced diagram $\mathcal{T} \equiv \mathcal{G}/\mathcal{S}$ of a self-energy subdiagram \mathcal{S} of the diagram \mathcal{G} . In this case we run into two kinds of IR divergence. One arises when a self-energy subdiagram \mathcal{S} behaves as a self-mass term. The standard mass-renormalization on \mathcal{G} subtracts $\delta m_{\mathcal{S}}M_{G/\mathcal{S}(i^*)}$ from M_G while $K_{\mathcal{S}}$ operation of Eq. (15) subtracts $\delta m_{\mathcal{S}}^{\text{UV}}M_{G/\mathcal{S}(i^*)}$. Thus, after subtraction by the $K_{\mathcal{S}}$ operation, we are left with $(\delta m_{\mathcal{S}} - \delta m_{\mathcal{S}}^{\text{UV}})M_{G/\mathcal{S}(i^*)}$, which has a linear IR divergence because of divergent $M_{G/\mathcal{S}(i^*)}$, except when $\delta m_{\mathcal{S}} = \delta m_{\mathcal{S}}^{\text{UV}}$. The easiest way to deal with this problem is to subtract $\delta m_{\mathcal{S}}$ entirely instead of only $\delta m_{\mathcal{S}}^{\text{UV}}$. We call this R -subtraction, which is incorporated in GENCODE N .

The other IR divergence occurs when a self-energy-like subdiagram \mathcal{S} behaves as a magnetic moment amplitude. The remaining diagram \mathcal{T} can be mimicked by a vertex diagram by shrinking the subdiagram \mathcal{S} to a point. This divergence is only logarithmic and the subtraction term can be constructed by applying the I -subtraction $\mathbb{I}_{\mathcal{T}}$ on the UV-finite amplitude $\underline{M}_{\mathcal{G}}$, which is shown to factorize as [20]

$$\mathbb{I}_{\mathcal{T}}\underline{M}_{\mathcal{G}} = L_{\mathcal{T}}^{\text{R}}\underline{M}_{\mathcal{S}}, \quad (16)$$

where $L_{\mathcal{T}}^{\text{R}}$ is the part of the vertex renormalization constant $L_{\mathcal{T}}$ that remains after all UV-divergent pieces are subtracted out.

These operations, carried out for all divergent subdiagrams of the unrenormalized integral $M_{\mathcal{G}}$, create a UV-finite and IR-finite integral $\Delta M_{\mathcal{G}}$. For a full account of these operations see Refs. [19, 20].

Since this scheme is different from the standard on-the-mass-shell renormalization, it is necessary to make an adjustment, called residual renormalization, which accounts for the difference of the standard renormalization and the UV-divergent (and IR-divergent) parts generated by K -operation (and I/R -subtractions).

The residual renormalization terms of individual diagrams must then be summed up over all diagrams involved. As the order of perturbation increases the total number of terms contributing to the residual renormalization increases rapidly so that it will become harder and harder to manage. Fortunately, the sum of all residual terms can be expressed concisely in terms of magnetic moments and finite parts of renormalization constants of lower orders, whose structure is closely related to that of the standard on-the-mass-shell renormalization. This observation enables us to obtain the sum of residual renormalization terms of all integrals starting from the expression of the standard renormalization. This approach is described in detail in Appendix A for the eighth-order $g-2$ after simpler cases of fourth- and sixth-orders are described for illustration of our method.

Since diagrams of Set IV are obtained from the magnetic moment contribution M_8 of 518 eighth-order vertices of four-photon-exchange type by inserting a second-order vacuum-polarization subdiagram in all possible ways, the residual renormalization term of the Set IV is readily derived from that of the residual renormalization term of M_8 . Namely, insertion of a closed loop of the lepton l_2 in the internal photon lines of Group V diagrams of lepton l_1 given in Eq. (A35) in all possible ways leads to the renormalized contribution of Set IV

to the lepton $g-2$ of the form:

$$\begin{aligned}
A^{(10)}[\text{Set IV}^{(l_1 l_2)}] &= \Delta M_{8,P_2}^{(l_1 l_2)} \\
&- 5\Delta M_{6,P_2}^{(l_1 l_2)} \Delta LB_2 \\
&- 5\Delta M_6 \Delta LB_{2,P_2}^{(l_1 l_2)} \\
&+ \Delta M_{4,P_2}^{(l_1 l_2)} (-3\Delta LB_4 + 9(\Delta LB_2)^2) \\
&+ \Delta M_4 (-3\Delta LB_{4,P_2}^{(l_1 l_2)} + 18\Delta LB_2 \Delta LB_{2,P_2}^{(l_1 l_2)}) \\
&+ M_{2,P_2}^{(l_1 l_2)} (-\Delta LB_6 + 6\Delta LB_4 \Delta LB_2 - 5(\Delta LB_2)^3) \\
&+ M_2 (-\Delta LB_{6,P_2}^{(l_1 l_2)} + 6\Delta LB_{4,P_2}^{(l_1 l_2)} \Delta LB_2 \\
&\quad + 6\Delta LB_4 \Delta LB_{2,P_2}^{(l_1 l_2)} - 15(\Delta LB_2)^2 \Delta LB_{2,P_2}^{(l_1 l_2)}) \\
&+ M_{2,P_2}^{(l_1 l_2)} \Delta \delta m_4 (4\Delta L_{2^*} + \Delta B_{2^*}) \\
&+ M_2 \Delta \delta m_{4,P_2}^{(l_1 l_2)} (4\Delta L_{2^*} + \Delta B_{2^*}) \\
&+ M_2 \Delta \delta m_4 (4\Delta L_{2^*,P_2}^{(l_1 l_2)} + \Delta B_{2^*,P_2}^{(l_1 l_2)}), \tag{17}
\end{aligned}$$

where superscripts such as $(l_1 l_1)$ and $(l_2 l_2)$ are omitted for terms which are independent of rest mass. See Appendix A for the explanation of notations.

$\Delta M_{8,P_2}^{(l_1 l_2)}$ is the sum of 74 WT-summed integrals enhanced by the insertion of vacuum-polarization-loop. Each of these 74 integrals is finite by our construction. Individual terms of residual renormalization are also UV- and IR-finite by construction. Eq. (17) thus maintains that $A^{(10)}[\text{Set IV}^{(l_1 l_2)}]$, which represents the quantity renormalized in the standard manner, can be expressed as the sum of completely finite quantities, each of which can thus be integrated by numerical means.

We should like to emphasize that Eq. (17) is analytically exact and involves no approximation as far as the subtraction term factorizes exactly as in Eqs. (14), (15), and (16).

IV. NUMERICAL EVALUATION OF $A_1^{(10)}[\text{Set IV}]$

$\Delta M_{\alpha,P_2}$, which is made UV-finite by K -operation and IR-finite by I/R -subtractions, is integrated numerically by the adaptive Monte-Carlo integration routine VEGAS [34]. The result for $(l_1 l_2) = (ee)$ are listed in Tables I and II. Auxiliary quantities needed for carrying out the residual renormalization are listed in Table III. Notations are those of Eq. (17).

TABLE I: Contributions of diagrams $M_{01,P2}, \dots, M_{24,P2}$ of Set IV to a_e for $(l_1 l_2) = (ee)$. The multiplicity n_F is the number of vertex diagrams represented by the integral and is incorporated in the numerical value. First 50 iterations are carried out using 1×10^8 sampling points per iteration. The integrations are continued with 1×10^9 sampling points per iteration and iterated as given in the second number of the fifth column. The integrals $M_{12,P2}$, $M_{16,P2}$, and $M_{18,P2}$ are evaluated with quadruple precision. All other integrals are evaluated with double precision.

Integral	n_F	Value (Error) including n_F	Sampling per iteration	No. of iterations
$M_{01,P2}$	28	-0.509 62 (38)	$1 \times 10^8, 1 \times 10^9$	50, 180
$M_{02,P2}$	56	0.060 41 (98)	$1 \times 10^8, 1 \times 10^9$	50, 200
$M_{03,P2}$	28	0.829 28 (60)	$1 \times 10^8, 1 \times 10^9$	50, 200
$M_{04,P2}$	56	1.497 37 (126)	$1 \times 10^8, 1 \times 10^9$	50, 360
$M_{05,P2}$	56	0.130 36 (46)	$1 \times 10^8, 1 \times 10^9$	50, 180
$M_{06,P2}$	56	-1.084 60 (94)	$1 \times 10^8, 1 \times 10^9$	50, 220
$M_{07,P2}$	56	-1.178 02 (48)	$1 \times 10^8, 1 \times 10^9$	50, 180
$M_{08,P2}$	56	-1.415 81 (121)	$1 \times 10^8, 1 \times 10^9$	50, 360
$M_{09,P2}$	56	-0.011 71 (95)	$1 \times 10^8, 1 \times 10^9$	50, 360
$M_{10,P2}$	56	-0.816 12 (107)	$1 \times 10^8, 1 \times 10^9$	50, 360
$M_{11,P2}$	28	0.768 73 (48)	$1 \times 10^8, 1 \times 10^9$	50, 200
$M_{12,P2}$	28	-1.631 37 (37)	$1 \times 10^8, 1 \times 10^9$	50, 5
$M_{13,P2}$	56	-2.353 59 (45)	$1 \times 10^8, 1 \times 10^9$	50, 200
$M_{14,P2}$	56	0.685 64 (83)	$1 \times 10^8, 1 \times 10^9$	50, 200
$M_{15,P2}$	56	0.461 55 (43)	$1 \times 10^8, 1 \times 10^9$	50, 200
$M_{16,P2}$	56	1.763 95 (111)	$1 \times 10^8, 1 \times 10^9$	50, 025
$M_{17,P2}$	56	3.290 90 (120)	$1 \times 10^8, 1 \times 10^9$	50, 340
$M_{18,P2}$	56	-0.052 73 (53)	$1 \times 10^8, 1 \times 10^9$	50, 5
$M_{19,P2}$	28	-1.403 73 (6)	$1 \times 10^8, 1 \times 10^9$	50, 180
$M_{20,P2}$	56	0.856 32 (43)	$1 \times 10^8, 1 \times 10^9$	50, 180
$M_{21,P2}$	28	0.360 89 (5)	$1 \times 10^8, 1 \times 10^9$	50, 180
$M_{22,P2}$	56	-0.743 60 (46)	$1 \times 10^8, 1 \times 10^9$	50, 180
$M_{23,P2}$	56	-1.120 08 (90)	$1 \times 10^8, 1 \times 10^9$	50, 200
$M_{24,P2}$	56	0.870 63 (59)	$1 \times 10^8, 1 \times 10^9$	50, 200

Substituting these quantities in Eq. (17) we obtain

$$A_1^{(10)}[\text{Set IV}^{(ee)}] = -7.729\ 6 \quad (48).$$

V. NUMERICAL EVALUATION OF $A_2^{(10)}(m_e/m_\mu)$ AND $A_2^{(10)}(m_e/m_\tau)$

Once FORTRAN programs for mass-independent contributions are obtained, it is straightforward to evaluate the contribution of mass-dependent terms such as $A_2^{(10)}(m_e/m_\mu)$. We simply have to choose an appropriate rest mass for the loop fermion l_2 . The result for

TABLE II: Contributions of diagrams $M_{25,P_2}, \dots, M_{47,P_2}$ of Set IV to a_e for $(l_1 l_2) = (ee)$. The multiplicity n_F is the number of vertex diagrams represented by the integral and is incorporated in the numerical value. All integrals are evaluated with double precision.

Integral	n_F	Value (Error) including n_F	Sampling per iteration	No. of iterations
M_{25,P_2}	28	-0.696 52 (25)	$1 \times 10^8, 1 \times 10^9$	50, 180
M_{26,P_2}	28	-0.432 10 (51)	$1 \times 10^8, 1 \times 10^9$	50, 200
M_{27,P_2}	56	1.120 35 (87)	$1 \times 10^8, 1 \times 10^9$	50, 200
M_{28,P_2}	56	0.783 12 (94)	$1 \times 10^8, 1 \times 10^9$	50, 240
M_{29,P_2}	28	1.495 00 (92)	$1 \times 10^8, 1 \times 10^9$	50, 200
M_{30,P_2}	28	-0.850 74 (95)	$1 \times 10^8, 1 \times 10^9$	50, 200
M_{31,P_2}	28	2.297 81 (13)	$1 \times 10^8, 1 \times 10^9$	50, 180
M_{32,P_2}	56	-2.675 78 (35)	$1 \times 10^8, 1 \times 10^9$	50, 180
M_{33,P_2}	28	-0.960 21 (6)	$1 \times 10^8, 1 \times 10^9$	50, 180
M_{34,P_2}	56	-0.967 04 (34)	$1 \times 10^8, 1 \times 10^9$	50, 180
M_{35,P_2}	56	-0.796 99 (36)	$1 \times 10^8, 1 \times 10^9$	50, 180
M_{36,P_2}	56	1.171 39 (41)	$1 \times 10^8, 1 \times 10^9$	50, 180
M_{37,P_2}	28	0.709 94 (13)	$1 \times 10^8, 1 \times 10^9$	50, 180
M_{38,P_2}	28	0.247 72 (29)	$1 \times 10^8, 1 \times 10^9$	50, 200
M_{39,P_2}	56	-0.830 00 (30)	$1 \times 10^8, 1 \times 10^9$	50, 180
M_{40,P_2}	56	-0.499 07 (47)	$1 \times 10^8, 1 \times 10^9$	50, 200
M_{41,P_2}	28	-1.083 44 (71)	$1 \times 10^8, 1 \times 10^9$	50, 200
M_{42,P_2}	28	0.576 12 (76)	$1 \times 10^8, 1 \times 10^9$	50, 200
M_{43,P_2}	28	-1.074 51 (41)	$1 \times 10^8, 1 \times 10^9$	50, 200
M_{44,P_2}	56	1.919 47 (60)	$1 \times 10^8, 1 \times 10^9$	50, 200
M_{45,P_2}	28	0.011 51 (37)	$1 \times 10^8, 1 \times 10^9$	50, 200
M_{46,P_2}	28	-0.588 88 (73)	$1 \times 10^8, 1 \times 10^9$	50, 200
M_{47,P_2}	28	-0.102 58 (65)	$1 \times 10^8, 1 \times 10^9$	50, 200

$A_2^{(10)}(m_e/m_\mu)$ is listed in Tables IV and V. From these Tables and the additional data listed in Table VI we obtain

$$A_2^{(10)}[\text{Set IV}^{(em)}] = -0.011\ 36\ (7). \quad (19)$$

We have also computed the contribution of tau-particle loop $A_2^{(10)}(m_e/m_\tau)$, which we give without details:

$$A_2^{(10)}[\text{Set IV}^{(et)}] = -0.000\ 093\ 7\ (104). \quad (20)$$

The contribution of the muon loop (19) is about 0.13 % of the electron loop contribution (18), while the contribution of the tau-lepton loop (20) is much smaller than the uncertainty of (18) and hence completely negligible at present.

TABLE III: Residual renormalization constants needed for the calculation of $a_e^{(10)}$ [SetIV (ee)]. Notations are those of Eq. (17).

$\Delta M_{6,P2}$	1.014 060 (30)	ΔM_6	0.425 820 (14)
$\Delta M_{4,P2}$	-0.106 707...	ΔM_4	0.030 833...
$M_{2,P2}$	0.015 687...	M_2	0.5
$\Delta LB_{6,P2}$	0.351 54 (93)	ΔLB_6	0.100 86 (77)
$\Delta LB_{4,P2}$	-0.114 228 (17)	ΔLB_4	0.027 930 (27)
$\Delta \delta m_{4,P2}$	0.679 769 (15)	$\Delta \delta m_4$	1.906 340 (21)
$\Delta LB_{2,P2}$	0.063 399...	ΔLB_2	0.75
$\Delta L_{2^*,P2}$	-0.023 531...	ΔL_{2^*}	-0.75
$\Delta B_{2^*,P2}$	0.047 062...	ΔB_{2^*}	1.5

VI. CONTRIBUTION TO THE MUON $g-2$

The muon $g-2$ also receives contributions from the Set IV. The contributions coming from the electron loop $(l_1 l_2) = (me)$ are listed in Tables VII and VIII. Auxiliary quantities needed to carry out the residual renormalization are listed in Table VI. From these quantities we obtain

$$A_2^{(10)}[\text{Set IV}^{(me)}] = -38.79 \quad (17).$$

We also obtained the contribution of the tau-lepton loop $A_2^{(10)}(m_e/m_\tau)$. The result is listed in Tables IX and X. From these Tables and the additional data listed in Table VI we obtain

$$A_2^{(10)}[\text{Set IV}^{(mt)}] = -0.435 7 \quad (22).$$

Including the mass-independent contribution (18), the total contribution to the muon $g-2$ amounts to

$$A_2^{(10)}[\text{Set IV}^{(me+mm+mt)}] = -46.95 \quad (17). \quad (23)$$

VII. DISCUSSION

Since the reliability of the eighth-order term M_8 is crucial for the validity of our work on the Set IV, let us sketch briefly how we established the validity of M_8 . See Ref. [5] for detailed

TABLE IV: Contributions of diagrams $M_{01,P_2}, \dots, M_{24,P_2}$ of Set IV to a_e for $(l_1 l_2) = (em)$. The multiplicity n_F is the number of vertex diagrams represented by the integral and is incorporated in the numerical value. The integral M_{12,P_2} is evaluated with quadruple precision. All other integrals are evaluated with double precision.

Integral	n_F	Value (Error) including n_F	Sampling per iteration	No. of iterations
$M_{01,P_2}^{(em)}$	28	0.000 759 (3)	$1 \times 10^7, 1 \times 10^8$	100, 20
$M_{02,P_2}^{(em)}$	56	0.000 205 (8)	$1 \times 10^7, 1 \times 10^8$	100, 20
$M_{03,P_2}^{(em)}$	28	0.001 757 (6)	$1 \times 10^7, 1 \times 10^8$	100, 20
$M_{04,P_2}^{(em)}$	56	0.001 170 (15)	$1 \times 10^7, 1 \times 10^8$	100, 20
$M_{05,P_2}^{(em)}$	56	0.000 197 (7)	$1 \times 10^7, 1 \times 10^8$	100, 20
$M_{06,P_2}^{(em)}$	56	-0.001 845 (12)	$1 \times 10^7, 1 \times 10^8$	100, 20
$M_{07,P_2}^{(em)}$	56	-0.001 866 (5)	$1 \times 10^7, 1 \times 10^8$	100, 20
$M_{08,P_2}^{(em)}$	56	0.000 922 (11)	$1 \times 10^7, 1 \times 10^8$	100, 20
$M_{09,P_2}^{(em)}$	56	-0.001 077 (16)	$1 \times 10^7, 1 \times 10^8$	100, 20
$M_{10,P_2}^{(em)}$	56	-0.001 316 (9)	$1 \times 10^7, 1 \times 10^8$	100, 20
$M_{11,P_2}^{(em)}$	28	0.000 310 (3)	$1 \times 10^7, 1 \times 10^8$	100, 20
$M_{12,P_2}^{(em)}$	28	0.000 822 (1)	1×10^7	20
$M_{13,P_2}^{(em)}$	56	-0.001 434 (8)	$1 \times 10^7, 1 \times 10^8$	100, 20
$M_{14,P_2}^{(em)}$	56	0.000 301 (10)	$1 \times 10^7, 1 \times 10^8$	100, 20
$M_{15,P_2}^{(em)}$	56	0.000 141 (5)	$1 \times 10^7, 1 \times 10^8$	100, 20
$M_{16,P_2}^{(em)}$	56	0.000 920 (8)	$1 \times 10^7, 1 \times 10^8$	100, 20
$M_{17,P_2}^{(em)}$	56	0.002 263 (14)	$1 \times 10^7, 1 \times 10^8$	100, 20
$M_{18,P_2}^{(em)}$	56	0.000 285 (4)	$1 \times 10^7, 1 \times 10^8$	100, 20
$M_{19,P_2}^{(em)}$	28	-0.001 671 (1)	$1 \times 10^7, 1 \times 10^8$	100, 20
$M_{20,P_2}^{(em)}$	56	0.000 738 (12)	$1 \times 10^7, 1 \times 10^8$	100, 20
$M_{21,P_2}^{(em)}$	28	0.000 210 (1)	$1 \times 10^7, 1 \times 10^8$	100, 20
$M_{22,P_2}^{(em)}$	56	0.000 880 (8)	$1 \times 10^7, 1 \times 10^8$	100, 20
$M_{23,P_2}^{(em)}$	56	0.000 105 (27)	$1 \times 10^7, 1 \times 10^8$	100, 20
$M_{24,P_2}^{(em)}$	56	0.000 371 (11)	$1 \times 10^7, 1 \times 10^8$	100, 20

accounts. Our approach was to evaluate the diagrams contributing to M_8 in two independent ways. The first method is to apply the scheme formulated more than 30 years ago [33]. The revised numerical evaluation by this formulation was reported recently [4, 5]. The second approach relies on the FORTRAN codes written by the automatic code-generator GENCODE N [19, 20]. This method treats the self-mass renormalization terms and IR divergent terms differently from the first method so that they can be regarded as practically independent of each other. Comparison of the results of these two methods revealed that the first one

TABLE V: Contributions of diagrams $M_{24,P2}, \dots, M_{47,P2}$ of Set IV to a_e for $(l_1 l_2) = (em)$. The multiplicity n_F is the number of vertex diagrams represented by the integral and is incorporated in the numerical value. All integrals are evaluated with double precision.

Integral	n_F	Value (Error) including n_F	Sampling per iteration	No. of iterations
$M_{25,P2}^{(em)}$	28	-0.001 089 (4)	$1 \times 10^7, 1 \times 10^8$	100, 20
$M_{26,P2}^{(em)}$	28	0.000 247 (3)	$1 \times 10^7, 1 \times 10^8$	100, 20
$M_{27,P2}^{(em)}$	56	0.001 937 (15)	$1 \times 10^7, 1 \times 10^8$	100, 20
$M_{28,P2}^{(em)}$	56	0.000 000 (8)	$1 \times 10^7, 1 \times 10^8$	100, 20
$M_{29,P2}^{(em)}$	28	0.000 786 (10)	$1 \times 10^7, 1 \times 10^8$	100, 20
$M_{30,P2}^{(em)}$	28	0.000 014 (4)	$1 \times 10^7, 1 \times 10^8$	100, 20
$M_{31,P2}^{(em)}$	28	0.001 088 (3)	$1 \times 10^7, 1 \times 10^8$	100, 20
$M_{32,P2}^{(em)}$	56	-0.002 282 (9)	$1 \times 10^7, 1 \times 10^8$	100, 20
$M_{33,P2}^{(em)}$	28	0.000 774 (1)	$1 \times 10^7, 1 \times 10^8$	100, 20
$M_{34,P2}^{(em)}$	56	-0.001 448 (7)	$1 \times 10^7, 1 \times 10^8$	100, 20
$M_{35,P2}^{(em)}$	56	0.000 296 (8)	$1 \times 10^7, 1 \times 10^8$	100, 20
$M_{36,P2}^{(em)}$	56	0.001 241 (8)	$1 \times 10^7, 1 \times 10^8$	100, 20
$M_{37,P2}^{(em)}$	28	0.000 421 (3)	$1 \times 10^7, 1 \times 10^8$	100, 20
$M_{38,P2}^{(em)}$	28	0.000 563 (3)	$1 \times 10^7, 1 \times 10^8$	100, 20
$M_{39,P2}^{(em)}$	56	0.000 892 (5)	$1 \times 10^7, 1 \times 10^8$	100, 20
$M_{40,P2}^{(em)}$	56	0.000 409 (3)	$1 \times 10^7, 1 \times 10^8$	100, 20
$M_{41,P2}^{(em)}$	28	0.000 775 (7)	$1 \times 10^7, 1 \times 10^8$	100, 20
$M_{42,P2}^{(em)}$	28	0.000 079 (4)	$1 \times 10^7, 1 \times 10^8$	100, 20
$M_{43,P2}^{(em)}$	28	0.000 246 (11)	$1 \times 10^7, 1 \times 10^8$	100, 20
$M_{44,P2}^{(em)}$	56	0.000 546 (10)	$1 \times 10^7, 1 \times 10^8$	100, 20
$M_{45,P2}^{(em)}$	28	0.000 117 (2)	$1 \times 10^7, 1 \times 10^8$	100, 20
$M_{46,P2}^{(em)}$	28	0.000 674 (8)	$1 \times 10^7, 1 \times 10^8$	100, 20
$M_{47,P2}^{(em)}$	28	0.000 203 (4)	$1 \times 10^7, 1 \times 10^8$	100, 20

had a subtle inconsistency in the handling of some IR subtraction terms. Correcting this error we now have two independent evaluations of M_8 which agree with each other within the precision of numerical integration [5].

Although we have not shown the analytic equivalence of the two methods directly, we are fully convinced that they are indeed equivalent by proving that they agree to 13 or 14 digits (in double precision) at all arbitrarily chosen points in the domain of integration. Only last few digits disagree due to difference in rounding off.

The validity of integrals of Set IV relies on the fact that two versions of M_8 agree com-

TABLE VI: Residual renormalization constants needed for the calculation of the mass-dependent contributions from Set IV diagrams. Notations are those of Eq. (17).

$\Delta M_{6,P2}^{(em)}$	0.000 721 65 (94)	$\Delta M_{4,P2}^{(em)}$	-0.000 018 910 (26)
$M_{2,P2}^{(em)}$	0.000 000 519 762 (21)		
$\Delta LB_{6,P2}^{(em)}$	0.000 705 (12)	$\Delta LB_{4,P2}^{(em)}$	-0.000 079 83 (10)
$\Delta \delta m_{4,P2}^{(em)}$	0.000 255 64 (5)	$\Delta LB_{2,P2}^{(em)}$	0.000 009 405 25 (83)
$\Delta L_{2^*,P2}^{(em)}$	-0.000 000 779 612 (11)	$\Delta B_{2^*,P2}^{(em)}$	0.000 001 559 224 (19)
$\Delta M_{6,P2}^{(me)}$	5.374 0 (45)	$\Delta M_{4,P2}^{(me)}$	-0.628 832...
$M_{2,P2}^{(me)}$	1.094 258...		
$\Delta LB_{6,P2}^{(me)}$	1.476 3 (33)	$\Delta LB_{4,P2}^{(me)}$	-0.308 75 (32)
$\Delta \delta m_{4,P2}^{(me)}$	11.151 39 (32)	$\Delta LB_{2,P2}^{(me)}$	1.885 733 (16)
$\Delta L_{2^*,P2}^{(me)}$	-1.641 436 (54)	$\Delta B_{2^*,P2}^{(me)}$	3.282 872 (107)
$\Delta M_{6,P2}^{(mt)}$	0.038 01 (14)	$\Delta M_{4,P2}^{(mt)}$	-0.001 641 9 (18)
$M_{2,P2}^{(mt)}$	0.000 078 067 4 (31)		
$\Delta LB_{6,P2}^{(mt)}$	0.023 97 (29)	$\Delta LB_{4,P2}^{(mt)}$	-0.004 155 7 (45)
$\Delta \delta m_{4,P2}^{(mt)}$	0.015 483 (25)	$\Delta LB_{2,P2}^{(mt)}$	0.000 831 107 (75)
$\Delta L_{2^*,P2}^{(mt)}$	-0.000 117 097 0 (15)	$\Delta B_{2^*,P2}^{(mt)}$	0.000 234 (1)

pletely with each other. As was noted in Sec. II we actually used only the second version of M_8 to build integrals of tenth-order diagrams of Set IV, because of a technical problem in the first version. However, we are convinced that the integrals of Set IV are indeed bug-free.

As is seen from (21) the contribution of Set IV to the muon $g-2$ is sizable, which is not unexpected. This is because the order of magnitude of the contribution of the dominant (me) term can be readily estimated, noting that the leading $\ln(m_\mu/m_e)$ term is determined by the charge renormalization procedure. This leads to

$$A_2^{(10)}[\text{Set IV}^{(me)}] \sim 4K_2 a_e^{(8)}[\text{Group V}] \sim -31.0 \quad (24)$$

where the factor 4 comes from the number of virtual photon lines of $a_e^{(8)}[\text{Group V}]$ into which a vacuum-polarization loop can be inserted, $a_e^{(8)}[\text{Group V}] \simeq -2.179 (3)$ [4, 5], and

TABLE VII: Contributions of diagrams $M_{01,P2}, \dots, M_{24,P2}$ of Set IV to a_μ for $(l_1 l_2) = (me)$. The multiplicity n_F is the number of vertex diagrams represented by the integral and is incorporated in the numerical value. The integrals $M_{12,P2}$, $M_{16,P2}$, and $M_{18,P2}$ are evaluated with quadruple precision. All other integrals are evaluated with double precision.

Integral	n_F	Value (Error) including n_F	Sampling per iteration	No. of iterations
$M_{01,P2}^{(me)}$	28	-0.369 5 (130)	$1 \times 10^8, 1 \times 10^9$	80, 48
$M_{02,P2}^{(me)}$	56	-8.223 2 (308)	$1 \times 10^8, 1 \times 10^9$	80, 140
$M_{03,P2}^{(me)}$	28	-3.986 6 (230)	$1 \times 10^8, 1 \times 10^9$	80, 80
$M_{04,P2}^{(me)}$	56	46.429 2 (587)	$1 \times 10^8, 1 \times 10^9$	80, 156
$M_{05,P2}^{(me)}$	56	19.803 9 (105)	$1 \times 10^8, 1 \times 10^9$	80, 48
$M_{06,P2}^{(me)}$	56	-11.614 8 (211)	$1 \times 10^8, 1 \times 10^9$	80, 80
$M_{07,P2}^{(me)}$	56	-0.558 3 (129)	$1 \times 10^8, 1 \times 10^9$	80, 72
$M_{08,P2}^{(me)}$	56	-48.877 7 (420)	$1 \times 10^8, 1 \times 10^9$	80, 130
$M_{09,P2}^{(me)}$	56	4.817 2 (310)	$1 \times 10^8, 1 \times 10^9$	80, 140
$M_{10,P2}^{(me)}$	56	18.291 5 (459)	$1 \times 10^8, 1 \times 10^9$	80, 156
$M_{11,P2}^{(me)}$	28	21.337 7 (299)	$1 \times 10^8, 1 \times 10^9$	80, 100
$M_{12,P2}^{(me)}$	28	-56.967 6 (174)	$1 \times 10^8, 1 \times 10^9$	50, 20
$M_{13,P2}^{(me)}$	56	-61.803 8 (142)	$1 \times 10^8, 1 \times 10^9$	80, 48
$M_{14,P2}^{(me)}$	56	21.147 2 (238)	$1 \times 10^8, 1 \times 10^9$	80, 80
$M_{15,P2}^{(me)}$	56	7.639 9 (138)	$1 \times 10^8, 1 \times 10^9$	80, 72
$M_{16,P2}^{(me)}$	56	62.954 8 (414)	$1 \times 10^8, 1 \times 10^9$	50, 35
$M_{17,P2}^{(me)}$	56	62.823 6 (412)	$1 \times 10^8, 1 \times 10^9$	80, 156
$M_{18,P2}^{(me)}$	56	-44.191 1 (207)	$1 \times 10^8, 1 \times 10^9$	50, 30
$M_{19,P2}^{(me)}$	28	-12.057 1 (14)	$1 \times 10^8, 1 \times 10^9$	80, 40
$M_{20,P2}^{(me)}$	56	9.281 7 (84)	$1 \times 10^8, 1 \times 10^9$	80, 48
$M_{21,P2}^{(me)}$	28	4.359 0 (12)	$1 \times 10^8, 1 \times 10^9$	80, 40
$M_{22,P2}^{(me)}$	56	-2.934 2 (105)	$1 \times 10^8, 1 \times 10^9$	80, 48
$M_{23,P2}^{(me)}$	56	-44.431 4 (185)	$1 \times 10^8, 1 \times 10^9$	80, 72
$M_{24,P2}^{(me)}$	56	19.396 5 (175)	$1 \times 10^8, 1 \times 10^9$	80, 72

the enhancement factor [3]

$$K_2 \sim \frac{2}{3} \ln(m_\mu/m_e) \sim 3.6 . \quad (25)$$

The value (24) may be regarded as a fair approximation to (21).

By now we have evaluated the complete set of tenth-order diagrams containing vacuum-polarization subdiagrams [3, 21–27]. (Note that the remaining Sets have no vacuum-polarization loop.) In particular its (me) contribution to the muon $g-2$, namely all sets

TABLE VIII: Contributions of diagrams $M_{25,P2}, \dots, M_{47,P2}$ of Set IV to a_μ for $(l_1 l_2) = (me)$. The multiplicity n_F is the number of vertex diagrams represented by the integral and is incorporated in the numerical value. All integrals are evaluated with double precision.

Integral	n_F	Value (Error) including n_F	Sampling per iteration	No. of iterations
$M_{25,P2}^{(me)}$	28	-1.148 1 (73)	$1 \times 10^8, 1 \times 10^9$	80, 40
$M_{26,P2}^{(me)}$	28	-13.572 5 (177)	$1 \times 10^8, 1 \times 10^9$	80, 80
$M_{27,P2}^{(me)}$	56	11.510 8 (246)	$1 \times 10^8, 1 \times 10^9$	80, 80
$M_{28,P2}^{(me)}$	56	36.510 0 (394)	$1 \times 10^8, 1 \times 10^9$	80, 156
$M_{29,P2}^{(me)}$	28	36.421 2 (298)	$1 \times 10^8, 1 \times 10^9$	80, 88
$M_{30,P2}^{(me)}$	28	-43.675 1 (402)	$1 \times 10^8, 1 \times 10^9$	80, 156
$M_{31,P2}^{(me)}$	28	35.547 0 (22)	$1 \times 10^8, 1 \times 10^9$	80, 40
$M_{32,P2}^{(me)}$	56	-30.768 6 (60)	$1 \times 10^8, 1 \times 10^9$	80, 40
$M_{33,P2}^{(me)}$	28	-14.328 3 (11)	$1 \times 10^8, 1 \times 10^9$	80, 40
$M_{34,P2}^{(me)}$	56	8.112 3 (66)	$1 \times 10^8, 1 \times 10^9$	80, 40
$M_{35,P2}^{(me)}$	56	-7.263 8 (65)	$1 \times 10^8, 1 \times 10^9$	80, 40
$M_{36,P2}^{(me)}$	56	3.414 7 (87)	$1 \times 10^8, 1 \times 10^9$	80, 48
$M_{37,P2}^{(me)}$	28	7.820 6 (24)	$1 \times 10^8, 1 \times 10^9$	80, 40
$M_{38,P2}^{(me)}$	28	-16.252 5 (81)	$1 \times 10^8, 1 \times 10^9$	80, 48
$M_{39,P2}^{(me)}$	56	-7.644 5 (78)	$1 \times 10^8, 1 \times 10^9$	80, 40
$M_{40,P2}^{(me)}$	56	2.819 0 (158)	$1 \times 10^8, 1 \times 10^9$	80, 72
$M_{41,P2}^{(me)}$	28	-25.777 5 (194)	$1 \times 10^8, 1 \times 10^9$	80, 72
$M_{42,P2}^{(me)}$	28	26.504 0 (291)	$1 \times 10^8, 1 \times 10^9$	80, 88
$M_{43,P2}^{(me)}$	28	-29.852 0 (100)	$1 \times 10^8, 1 \times 10^9$	80, 48
$M_{44,P2}^{(me)}$	56	37.460 8 (173)	$1 \times 10^8, 1 \times 10^9$	80, 72
$M_{45,P2}^{(me)}$	28	9.735 1 (173)	$1 \times 10^8, 1 \times 10^9$	80, 72
$M_{46,P2}^{(me)}$	28	8.399 9 (213)	$1 \times 10^8, 1 \times 10^9$	80, 80
$M_{47,P2}^{(me)}$	28	-22.410 1 (284)	$1 \times 10^8, 1 \times 10^9$	80, 104

excluding light-by-light scattering loops, is given by

$$A_2^{(10)}[\text{All sets excluding l-l loops}]^{(me)} \simeq 48.88 \quad (26)$$

This may be compared with the corresponding result $\Delta_{(10)}^{(I)} \simeq 32$ obtained by an estimate based on the renormalization group method [35].

TABLE IX: Contributions of diagrams $M_{01,P_2}, \dots, M_{24,P_2}$ of Set IV to a_μ for $(l_1 l_2) = (mt)$. The multiplicity n_F is the number of vertex diagrams represented by the integral and is incorporated in the numerical value. The integral M_{12,P_2} is evaluated with quadruple precision. All other integrals are evaluated with double precision.

Integral	n_F	Value (Error) including n_F	Sampling per iteration	No. of iterations
$M_{01,P_2}^{(mt)}$	28	-0.026 89 (15)	1×10^7	100
$M_{02,P_2}^{(mt)}$	56	-0.002 06 (37)	1×10^7	100
$M_{03,P_2}^{(mt)}$	28	0.051 83 (23)	1×10^7	100
$M_{04,P_2}^{(mt)}$	56	0.049 99 (55)	1×10^7	100
$M_{05,P_2}^{(mt)}$	56	-0.011 20 (29)	1×10^7	100
$M_{06,P_2}^{(mt)}$	56	-0.060 08 (52)	1×10^7	100
$M_{07,P_2}^{(mt)}$	56	-0.065 38 (24)	1×10^7	100
$M_{08,P_2}^{(mt)}$	56	-0.038 51 (55)	1×10^7	100
$M_{09,P_2}^{(mt)}$	56	-0.026 52 (62)	1×10^7	100
$M_{10,P_2}^{(mt)}$	56	-0.050 11 (44)	1×10^7	100
$M_{11,P_2}^{(mt)}$	28	0.016 61 (16)	1×10^7	100
$M_{12,P_2}^{(mt)}$	28	-0.037 85 (2)	1×10^7	50
$M_{13,P_2}^{(mt)}$	56	-0.060 34 (30)	1×10^7	100
$M_{14,P_2}^{(mt)}$	56	0.000 86 (43)	1×10^7	100
$M_{15,P_2}^{(mt)}$	56	0.009 38 (23)	1×10^7	100
$M_{16,P_2}^{(mt)}$	56	0.040 26 (49)	1×10^7	100
$M_{17,P_2}^{(mt)}$	56	0.101 13 (62)	1×10^7	100
$M_{18,P_2}^{(mt)}$	56	0.011 93 (28)	1×10^7	100
$M_{19,P_2}^{(mt)}$	28	-0.063 10 (5)	1×10^7	100
$M_{20,P_2}^{(mt)}$	56	0.029 21 (37)	1×10^7	100
$M_{21,P_2}^{(mt)}$	28	0.007 11 (4)	1×10^7	100
$M_{22,P_2}^{(mt)}$	56	-0.034 71 (33)	1×10^7	100
$M_{23,P_2}^{(mt)}$	56	-0.008 27 (68)	1×10^7	100
$M_{24,P_2}^{(mt)}$	56	0.022 23 (39)	1×10^7	100

Acknowledgments

This work is supported in part by the JSPS Grant-in-Aid for Scientific Research (C)19540322, (C)23540331, and (C)20540261. T. K.'s work is supported in part by the U. S. National Science Foundation under Grant NSF-PHY-0757868, and the International Exchange Support Grants (FY2010) of RIKEN. T. K. thanks RIKEN for the hospitality extended to him while a part of this work was carried out. Numerical calculations are

TABLE X: Contributions of diagrams $M_{25,P_2}, \dots, M_{47,P_2}$ of Set IV to a_μ for $(l_1 l_2) = (mt)$. The multiplicity n_F is the number of vertex diagrams represented by the integral and is incorporated in the numerical value. All integrals are evaluated with double precision.

Integral	n_F	Value (Error) including n_F	Sampling per iteration	No. of iterations
$M_{25,P_2}^{(mt)}$	28	-0.039 19 (15)	1×10^7	100
$M_{26,P_2}^{(mt)}$	28	-0.010 15 (17)	1×10^7	100
$M_{27,P_2}^{(mt)}$	56	0.060 33 (53)	1×10^7	100
$M_{28,P_2}^{(mt)}$	56	0.006 03 (36)	1×10^7	100
$M_{29,P_2}^{(mt)}$	28	0.037 86 (34)	1×10^7	100
$M_{30,P_2}^{(mt)}$	28	-0.005 19 (24)	1×10^7	100
$M_{31,P_2}^{(mt)}$	28	0.056 43 (12)	1×10^7	100
$M_{32,P_2}^{(mt)}$	56	-0.096 26 (30)	1×10^7	100
$M_{33,P_2}^{(mt)}$	28	-0.030 72 (5)	1×10^7	100
$M_{34,P_2}^{(mt)}$	56	-0.060 57 (25)	1×10^7	100
$M_{35,P_2}^{(mt)}$	56	-0.025 98 (31)	1×10^7	100
$M_{36,P_2}^{(mt)}$	56	0.050 76 (32)	1×10^7	100
$M_{37,P_2}^{(mt)}$	28	0.019 70 (10)	1×10^7	100
$M_{38,P_2}^{(mt)}$	28	0.021 52 (14)	1×10^7	100
$M_{39,P_2}^{(mt)}$	56	-0.034 44 (21)	1×10^7	100
$M_{40,P_2}^{(mt)}$	56	-0.018 44 (21)	1×10^7	100
$M_{41,P_2}^{(mt)}$	28	-0.033 08 (28)	1×10^7	100
$M_{42,P_2}^{(mt)}$	28	0.006 74 (25)	1×10^7	100
$M_{43,P_2}^{(mt)}$	28	-0.016 64 (36)	1×10^7	100
$M_{44,P_2}^{(mt)}$	56	0.039 39 (35)	1×10^7	100
$M_{45,P_2}^{(mt)}$	28	0.002 23 (14)	1×10^7	100
$M_{46,P_2}^{(mt)}$	28	-0.028 76 (34)	1×10^7	100
$M_{47,P_2}^{(mt)}$	28	-0.004 02 (21)	1×10^7	100

conducted on the RIKEN Super Combined Cluster System (RSCC) and the RIKEN Integrated Cluster of Clusters (RICC) supercomputing systems. Special thanks are due to late Dr. T. Shigetani and High Performance Computing group of RIKEN's Advanced Center for Computing and Communication.

Appendix A: Summing up Residual Renormalization Terms

The purpose of this Appendix is to obtain the sum of residual renormalization terms of the Set IV. Since diagrams of Set IV have exact correspondence with the diagrams of Group V of the *eighth-order* $g-2$, however, it is simpler to consider the residual renormalization of the diagrams of Group V, from which the residual renormalization of the Set IV can be readily derived.

In our approach integrals of individual diagrams must be made convergent before they are integrated numerically. This is achieved by constructing terms which subtract UV-divergent parts by K -operation and IR-divergent parts by I/R -subtractions. Since this scheme is different from the standard on-shell renormalization, it is necessary to make an adjustment, called residual renormalization. Residual renormalization terms of individual diagrams must then be summed up over all diagrams involved.

As the order of perturbation increases the total number of terms contributing to the residual renormalization increases rapidly so that it will become harder and harder to manage. Fortunately the sum of all residual terms can be expressed concisely in terms of magnetic moments and finite parts of renormalization constants of lower orders [5], and the sum has a structure closely related to that of the standard on-shell renormalization. This enables us to confirm the validity of the sum of residual renormalization terms starting from the expression of the standard renormalization.

To see this relation clearly it is useful to treat UV-divergence and IR-divergence separately. We present the logic of our approach for the fourth-, sixth-, and eighth-order cases, in that order. We deal here only with Ward-Takahashi(WT)-summed diagrams of q -type, namely diagrams without closed lepton loops. Thus M_{2n} and a_{2n} , $n = 1, 2, \dots$, refer to unrenormalized and renormalized amplitudes of such diagrams, respectively.

Our discussion here follows the scheme incorporated in the automatic code generator GENCODE N , which is applicable to any value of the order N .

1. fourth-order case

The standard renormalization of the fourth-order magnetic moment a_4 can be expressed in the form

$$a_4 = M_4 - 2L_2M_2 - B_2M_2 - \delta m_2M_{2^*}, \quad (\text{A1})$$

where M_2 is the second-order magnetic moment, M_{2^*} is obtained from M_2 by inserting a two-point vertex in the lepton line of M_2 , and M_4 is the sum of unrenormalized WT-summed amplitudes M_{4a} and M_{4b} :

$$M_4 \equiv M_{4a} + M_{4b}, \quad (\text{A2})$$

where $4a$ and $4b$ refer to the fourth-order diagrams in which two virtual photons are crossed and uncrossed, respectively. The coefficients of renormalization constants L_2 and B_2 in Eq. (A1) reflect the fact that M_{4a} is obtained by inserting a second-order vertex diagram in two vertices of M_2 and M_{4b} is obtained by inserting a second-order self-energy diagram in the electron line of M_2 .

a. Separation of UV divergences by the K -operation

M_4 has no *overall* UV divergence. However, it has UV divergences coming from subdiagrams. Applying K -operation on these divergences we obtain

$$M_4 = B_2^{\text{UV}}M_2 + \delta m_2^{\text{UV}}M_{2^*} + 2L_2^{\text{UV}}M_2 + M_4^{\text{R}}, \quad (\text{A3})$$

where the superscript R in M_4^{R} means that all subdiagram UV divergences are removed from M_4 . L_2^{UV} and B_2^{UV} are the UV-divergent parts separated out from L_2 and B_2 by the K -operation and L_2^{R} and B_2^{R} are UV-finite (but IR-divergent) remainders:

$$\begin{aligned} L_2 &= L_2^{\text{UV}} + L_2^{\text{R}}, \\ B_2 &= B_2^{\text{UV}} + B_2^{\text{R}}, \\ \delta m_2 &= \delta m_2^{\text{UV}}. \end{aligned} \quad (\text{A4})$$

$\delta m_2^{\text{R}} = 0$ is the specific feature of the K -operation for the second-order self-energy diagram.

Substituting Eqs. (A3) and (A4) in Eq. (A1) we obtain

$$a_4 = M_4^{\text{R}} - M_2(2L_2^{\text{R}} + B_2^{\text{R}}), \quad (\text{A5})$$

Note that the coefficients of L_2^R and B_2^R in Eq. (A5) inherit the coefficients of L_2 and B_2 in Eq. (A1).

b. Separation of IR divergences by the I/R-subtraction

The second-order mass renormalization is completely carried out and no remainder is left in the K -operation. The R -subtraction, then, is not applied by GENCODEN in the case of the fourth order. IR divergence is caused by a photon spanning over a self-energy-like subdiagram which actually represents a lower-order magnetic moment. This magnetic moment can be effectively represented by a three-point vertex between one photon and two electrons. Thus, the UV-finite term M_4^R must have an IR singular structure which is similar to that of the vertex renormalization constant L_2^R :

$$M_4^R = M_2 L_2^R + \Delta M_4, \quad (\text{A6})$$

where M_2 comes from the second-order self-energy subdiagram of M_{4b} and L_2^R appears by replacing the M_2 self-energy subdiagram by a point vertex.

The IR-divergence is also found in the vertex and wave-function renormalization constants. The WT-identity

$$L_2 + B_2 = 0 \quad (\text{A7})$$

guarantees that L_2 and B_2 have the same, but opposite in sign, IR singularity. This enables us to separate the IR-singular and finite terms of L_2^R and B_2^R as follows:

$$\begin{aligned} L_2^R &= I_2 + \Delta L_2, \\ B_2^R &= -I_2 + \Delta B_2. \end{aligned} \quad (\text{A8})$$

where I_2 is IR-singular but its finite part is undetermined. The finite terms ΔL_2 and ΔB_2 depend on how we define I_2 . For instance, in Ref. [32], the I -operation was defined so that $I_2 = L_2^R = \ln(\lambda/m) + 5/4$, where λ is the photon mass. The sum $L_2^R + B_2^R$, however, does not depend on the definition of I_2 . We find that

$$\Delta L B_2 \equiv L_2^R + B_2^R = \Delta L_2 + \Delta B_2 = \frac{3}{4}. \quad (\text{A9})$$

In other words, the finite quantity $\Delta L B_2$ is determined by how we extract UV divergence by the K -operation from each of L_2 and B_2 :

$$L_2^{\text{UV}} + B_2^{\text{UV}} = -\frac{3}{4}. \quad (\text{A10})$$

Substituting Eqs. (A6) and (A8) in Eq. (A5), one can express a_4 defined by the standard renormalization as a sum of finite terms only:

$$a_4 = \Delta M_4 - M_2 \Delta L B_2. \quad (\text{A11})$$

2. sixth-order case

The sixth-order magnetic moment a_6 has contributions from ten diagrams, each of which represents the sum of five vertex diagrams transformed with the help of the WT-identity. In the standard renormalization it can be written in terms of unrenormalized amplitudes M_6 , M_4 , etc., and various renormalization constants as

$$\begin{aligned} a_6 &= M_6 \\ &- M_4(3B_2 + 4L_2) - M_{4^*}\delta m_2 \\ &- M_2(B_4 + 2L_4) - M_{2^*}\delta m_4 \\ &+ M_2\{2(B_2)^2 + 8B_2L_2 + 7(L_2)^2\} + M_{2^*}(3B_2 + 4L_2)\delta m_2 \\ &+ M_2(B_{2^*} + 4L_{2^*})\delta m_2 \\ &+ M_{2^*}\delta m_2\delta m_{2^*} + M_{2^{**}}(\delta m_2)^2, \end{aligned} \quad (\text{A12})$$

where M_4 is defined by Eq. (A2), $M_{2^{**}}$ is obtained from M_2 by inserting two two-point vertices in the lepton line of M_2 , and

$$\begin{aligned} M_6 &= \sum_{i=A}^H \eta_i M_{6i}, \quad \eta_i = 1 \text{ except that } \eta_D = \eta_G = 2, \\ M_{4^*} &= \sum_{i=1}^3 (M_{4a(i^*)} + M_{4b(i^*)}), \\ B_4 &= B_{4a} + B_{4b}, \\ L_4 &= \sum_{i=1}^3 (L_{4a(i)} + L_{4b(i)}), \\ \delta m_4 &= \delta m_{4a} + \delta m_{4b}. \end{aligned} \quad (\text{A13})$$

$M_{4a(i^*)}$ is obtained from M_{4a} (which contains three lepton lines 1, 2, 3) by inserting a two-point vertex in the lepton line i of M_{4a} , and $L_{4a(i)}$ is the vertex renormalization constant of the diagram in which an external vertex is inserted in the lepton line i of the diagram 4a. Similar notation is applied for the diagrams built from 4b.

The coefficient of M_4 in Eq. (A12) can be readily understood noting that the fourth-order self-energy diagrams M_{4a} and M_{4b} have three fermion lines into which second-order self-energy can be inserted and four vertices into which second-order vertex can be inserted. Similarly, there are one fermion line and two vertices in the second-order self-energy diagram M_2 into which we can insert a B_4 or a L_4 , which leads to $-M_2(B_4 + 2L_4)$. The term $M_2\{2(B_2)^2 + 8B_2L_2 + 7(L_2)^2\}$ comes from two ways of inserting B_2 in M_2 (one disjoint and one nested relations of two B_2 's [19]), eight ways of inserting one L_2 and one B_2 in M_2 (two disjoint, two overlapping, and four nested relations of L_2 and B_2), and seven ways of inserting two L_2 in M_2 (one disjoint, four overlapping, and two nested relations of two L_2 's). There is only one way to insert δm_4 in M_2 and δm_2 in B_2 of M_2B_2 . There are three ways to insert δm_2 in M_4 , but the coefficient three is included in the definition of M_{4*} . There are four ways to insert δm_2 in L_2 of M_2L_2 . The coefficients of other terms can be understood in a similar fashion.

a. Separation of UV divergences by the K-operation

Analysis of the UV divergence structure of M_6 , L_4 , B_4 , and δm_4 by the K -operation leads to

$$\begin{aligned}
M_6 &= M_6^R \\
&+ M_4(3B_2^{\text{UV}} + 4L_2^{\text{UV}}) + M_{4*}\delta m_2 \\
&+ M_2(B_4^{\text{UV}} + 2L_4^{\text{UV}}) + M_{2*}\delta m_4^{\text{UV}} \\
&- M_2\{(B_2^{\text{UV}})^2 + B_2^{\text{UV}}B_{2'}^{\text{UV}} + 4B_2^{\text{UV}}L_2^{\text{UV}} + 4B_2^{\text{UV}}L_{2'}^{\text{UV}} + 7(L_2^{\text{UV}})^2\} \\
&- M_{2*}(2B_2^{\text{UV}} + 4L_2^{\text{UV}})\delta m_2 \\
&- M_{2*}B_2^{\text{UV}}\delta m_{2'}^{\text{UV}} \\
&- M_{2*}\delta m_{2*}^{\text{UV}}\delta m_2 \\
&- M_{2**}(\delta m_2)^2,
\end{aligned} \tag{A14}$$

where

$$M_6^R = \sum_{i=A}^H \eta_i M_{6i}^R, \quad \eta_i = 1 \text{ except that } \eta_D = \eta_G = 2, \tag{A15}$$

is the UV-finite part of M_6 . UV-divergent parts of L_4 , B_4 , and δm_4 are separated as follows:

$$\begin{aligned}
L_4 &= L_4^{\text{UV}} + 3L_2^{\text{UV}}L_2^{\text{R}} + 2B_2^{\text{UV}}L_2^{\text{R}} + 2\delta m_2L_{2^*} + L_4^{\text{R}}, \\
B_4 &= B_4^{\text{UV}} + 2L_2^{\text{UV}}B_2^{\text{R}} + B_2^{\text{UV}}B_2^{\text{R}} + \delta m_2B_{2^*} + B_4^{\text{R}}, \\
\delta m_4 &= \delta m_4^{\text{UV}} + \delta m_2\delta m_{2^*}^{\text{R}} + B_2^{\text{UV}}\delta m_{2^*}^{\text{R}} + \delta m_4^{\text{R}}.
\end{aligned} \tag{A16}$$

M_4^{R} is defined in Eq. (A3), and L_2^{UV} and B_2^{UV} are defined in Eq. (A4).

Substituting Eqs. (A14), (A3), (A16), and (A4) in Eq. (A12) in this order, we obtain a_6 expressed by UV-finite quantities only:

$$\begin{aligned}
a_6 &= M_6^{\text{R}} \\
&- M_4^{\text{R}}(3B_2^{\text{R}} + 4L_2^{\text{R}}) \\
&- M_2(B_4^{\text{R}} + 2L_4^{\text{R}}) - M_{2^*}\delta m_4^{\text{R}} \\
&+ M_2\{2(B_2^{\text{R}})^2 + 8B_2^{\text{R}}L_2^{\text{R}} + 7(L_2^{\text{R}})^2\}.
\end{aligned} \tag{A17}$$

Note that this equation has exactly the same structure as Eq. (A12), although it looks simpler because $\delta m_2^{\text{R}} = 0$ in the K -operation. This is what one would expect since, in Eq. (A12), all UV-divergent quantities must cancel out, leaving only UV-finite pieces with their original numerical coefficients.

b. Separation of IR divergences by the I/R-subtraction

Since Eq. (A17) has no linearly IR divergent term caused by the self-mass term, there is no need to invoke the R -subtraction. We, however, retain the R -subtraction that is incorporated in GENCODEN. Quantities obtained above can be expressed as the sum of logarithmically IR-divergent pieces defined by the I -subtraction and finite remainders together with the residual mass-renormalization term defined by the R -subtraction:

$$\begin{aligned}
M_6^{\text{R}} &= L_4^{\text{R}}M_2 - (L_2^{\text{R}})^2M_2 + L_2^{\text{R}}M_4^{\text{R}} + \delta m_4^{\text{R}}M_{2^*} + \Delta M_6, \\
L_4^{\text{R}} &= I_4 + (L_2^{\text{R}})^2 + \Delta L_4 \\
B_4^{\text{R}} &= -I_4 + L_2^{\text{R}}B_2^{\text{R}} + \Delta B_4,
\end{aligned} \tag{A18}$$

where IR-divergent terms are contained in L_2^{R} , B_2^{R} and I_4 term. The WT-identity guarantees that L_4 and B_4 have the same overall IR-divergence which we call I_4 . In the previous work

[32] the I_4 is chosen as the sum of non-contraction terms $I_{4a(i)}$ of the vertex renormalization constants $L_{4a(i)}$:

$$I_4 \equiv I_{4a(1)} + I_{4a(2)} + I_{4a(3)} + I_{4b(1)} + I_{4b(2)} + I_{4b(3)}. \quad (\text{A19})$$

The finite quantities ΔL_4 and ΔB_4 depend on how I_4 is defined. But the sum of $L_4^R + B_4^R$ is independent from the definition of I_4 . Therefore, we introduce the finite quantity ΔLB_4 by

$$\Delta LB_4 \equiv L_4^R + B_4^R - L_2^R \Delta LB_2 = \Delta L_4 + \Delta B_4. \quad (\text{A20})$$

Note that the value of ΔLB_4 is unambiguously determined by our choice of L_4^{UV} and B_4^{UV} in the K -operation and by the WT-identity $L_4 + B_4 = 0$.

Substituting Eqs. (A18), (A20), (A6), and (A9) in Eq. (A17) in this order, we obtain a_6 of standard renormalization as the sum of finite terms only

$$\begin{aligned} a_6 = & \Delta M_6 - 3\Delta M_4 \Delta LB_2 \\ & + M_2 \{-\Delta LB_4 + 2(\Delta LB_2)^2\}. \end{aligned} \quad (\text{A21})$$

3. eighth-order case

The eighth-order magnetic moment a_8 has contributions from 74 WT-summed diagrams. In the standard renormalization the renormalized moment a_8 can be written in terms of

unrenormalized amplitudes M_8 , M_6 , M_4 , etc., and various renormalization constants as

$$\begin{aligned}
a_8 = & M_8 \\
& - M_6(5B_2 + 6L_2) \\
& - M_{6^*}\delta m_2 \\
& + M_4\{-3B_4 - 4L_4 + 9(B_2)^2 + 26B_2L_2 + 18(L_2)^2 + \delta m_2(3B_{2^*} + 8L_{2^*})\} \\
& + M_{4^*}\{\delta m_2(5B_2 + 6L_2) + \delta m_2\delta m_{2^*} - \delta m_4\} \\
& + M_{4^{**}}(\delta m_2)^2 \\
& + M_2\{-B_6 - 2L_6 + 12L_4B_2 + 18L_4L_2 + 6B_4B_2 + 10B_4L_2 \\
& \quad - 54B_2(L_2)^2 - 30(B_2)^2L_2 - 5(B_2)^3 - 30(L_2)^3\} \\
& + M_2\delta m_4(B_{2^*} + 4L_{2^*}) \\
& + M_2\delta m_2(B_{4^*} + 2L_{4^*} - 6B_2B_{2^*} - 24B_2L_{2^*} - 10B_{2^*}L_2 - 36L_2L_{2^*}) \\
& - M_2\delta m_2\delta m_{2^*}(B_{2^*} + 4L_{2^*}) \\
& - M_2(\delta m_2)^2(B_{2^{**}} + 4L_{2^{**\dagger}} + 2L_{2^{\dagger*}}) \\
& + M_{2^*}\delta m_2\{3B_4 + 4L_4 + \delta m_{4^*} - 26B_2L_2 - 9(B_2)^2 - 18(L_2)^2\} \\
& - M_{2^*}\delta m_6 \\
& + M_{2^*}\delta m_4(5B_2 + 6L_2 + \delta m_{2^*}) \\
& - M_{2^*}(\delta m_2)^2(3B_{2^*} + 8L_{2^*} + \delta m_{2^{**}}) \\
& - M_{2^*}\delta m_2\delta m_{2^*}(5B_2 + 6L_2) \\
& - M_{2^*}\delta m_2(\delta m_{2^*})^2 \\
& + M_{2^{**}}\delta m_2\{2\delta m_4 - \delta m_2(5B_2 + 6L_2 + 2\delta m_{2^*})\} \\
& - M_{2^{***}}(\delta m_2)^3.
\end{aligned} \tag{A22}$$

M_8 is defined by

$$M_8 = \sum_{\alpha=01}^{47} \eta_\alpha M_\alpha, \tag{A23}$$

where $\eta_\alpha = 1$ for time-reversal-symmetric diagrams and $\eta_\alpha = 2$ for others.

a. Separation of UV divergences by the K-operation

The UV divergence structure of M_8 is given by

$$\begin{aligned}
M_8 &= M_8^{\text{R}} \\
&+ M_6(5B_2^{\text{UV}} + 6L_2^{\text{UV}}) \\
&+ M_{6^*}\delta m_2 \\
&+ M_4\{3B_4^{\text{UV}} + 4L_4^{\text{UV}} - 3B_2^{\text{UV}}B_{2'}^{\text{UV}} - 6(B_2^{\text{UV}})^2 - 18B_2^{\text{UV}}L_2^{\text{UV}} - 8B_2^{\text{UV}}L_{2'}^{\text{UV}} - 18(L_2^{\text{UV}})^2\} \\
&+ M_{4^*}(\delta m_4^{\text{UV}} - B_2^{\text{UV}}\delta m_{2'}^{\text{UV}} - 4\delta m_2B_2^{\text{UV}} - 6\delta m_2L_2^{\text{UV}} - \delta m_2\delta m_{2^*}^{\text{UV}}) \\
&- M_{4^{**}}(\delta m_2)^2 \\
&+ M_2\{B_6^{\text{UV}} + 2L_6^{\text{UV}} - 2B_4^{\text{UV}}B_2^{\text{UV}} - 6B_4^{\text{UV}}L_2^{\text{UV}} - B_4^{\text{UV}}B_{2'}^{\text{UV}} - 4B_4^{\text{UV}}L_{2'}^{\text{UV}} \\
&- 4L_4^{\text{UV}}B_2^{\text{UV}} - 18L_4^{\text{UV}}L_2^{\text{UV}} + 6B_2^{\text{UV}}L_2^{\text{UV}}B_{2'}^{\text{UV}} + 36B_2^{\text{UV}}L_2^{\text{UV}}L_{2'}^{\text{UV}} + 18B_2^{\text{UV}}(L_2^{\text{UV}})^2 \\
&- B_2^{\text{UV}}B_{4'}^{\text{UV}} - 2B_2^{\text{UV}}L_{4'}^{\text{UV}} + 4B_2^{\text{UV}}B_{2'}^{\text{UV}}L_{2'}^{\text{UV}} + B_2^{\text{UV}}(B_{2'}^{\text{UV}})^2 + 6(B_2^{\text{UV}})^2L_2^{\text{UV}} \\
&+ 2(B_2^{\text{UV}})^2L_{2''}^{\text{UV}} + (B_2^{\text{UV}})^2B_{2''}^{\text{UV}} + 2(B_2^{\text{UV}})^2B_{2'}^{\text{UV}} \\
&+ 8(B_2^{\text{UV}})^2L_{2'}^{\text{UV}} + (B_2^{\text{UV}})^3 + 30(L_2^{\text{UV}})^3\} \\
&+ M_{2^*}\{\delta m_6^{\text{UV}} - B_2^{\text{UV}}\delta m_{4'}^{\text{UV}} + (B_2^{\text{UV}})^2\delta m_{2''}^{\text{UV}}\} \\
&+ M_{2^*}\delta m_4^{\text{UV}}\{-2B_2^{\text{UV}} - 6L_2^{\text{UV}} - \delta m_{2^*}^{\text{UV}}\} \\
&+ M_{2^*}\delta m_{2'}^{\text{UV}}\{-B_4^{\text{UV}} + 6B_2^{\text{UV}}L_2^{\text{UV}} + 2(B_2^{\text{UV}})^2 + B_2^{\text{UV}}B_{2'}^{\text{UV}} + B_2^{\text{UV}}\delta m_{2^*}^{\text{UV}}\} \\
&+ M_{2^*}\delta m_2\{-2B_4^{\text{UV}} - 4L_4^{\text{UV}} - \delta m_{4^*}^{\text{UV}} + 18(L_2^{\text{UV}})^2 \\
&+ B_2^{\text{UV}}(12L_2^{\text{UV}} + 8L_{2'}^{\text{UV}} + 2B_{2'}^{\text{UV}} + 3B_2^{\text{UV}} + 2\delta m_{2^*'}^{\text{UV}}) \\
&+ \delta m_{2^*}^{\text{UV}}(2B_2^{\text{UV}} + 6L_2^{\text{UV}} + \delta m_{2^*}^{\text{UV}})\} \\
&+ M_{2^{**}}\delta m_2\{-2\delta m_4^{\text{UV}} + (3\delta m_2 + 2\delta m_{2'}^{\text{UV}})B_2^{\text{UV}} + 6\delta m_2L_2^{\text{UV}} + 2\delta m_2\delta m_{2^*}^{\text{UV}}\} \\
&+ M_{2^{***}}(\delta m_2)^3. \tag{A24}
\end{aligned}$$

The quantities with a prime, $L_{2'}$, called derivative amplitudes, arises from a fourth-order diagram that contains a self-energy subdiagram. This self-energy subdiagram supplies the inverse of the fermion propagator times the wave function renormalization constant and cancels out one of the adjacent fermion propagators and yields another renormalization constant L_2 . In the expression $L_{2'}$, the inverse fermion propagator and the adjacent fermion propagator are left in the numerator and denominator, respectively, of the Feynman parametric expression of the amplitude. Thus the whole renormalization constant $L_{2'}$ is analytically

identical with L_2 . But, the separation of UV divergence by the K -operation works differently in two cases, so that $L_{2'}^{\text{UV}}$ is different from L_2^{UV} by a finite amount.

A similar consideration applies to higher order quantities. Take, for instance, L_4 which consists of four fermion lines. There are four ways to insert a self-energy subdiagram to L_4 . Since we define $L_{4'}$ as the sum of all derivative amplitudes of L_4 , we have $L_{4'} = 4L_4$. Similarly, $B_{4'} = 3B_4$.

The second-order derivative amplitude, such as $L_{2'}$, however, does not include its symmetric factor in our definition. Thus, $L_{2'} = L_2$.

We also need the UV divergence structures of the renormalization terms B_6 , L_6 , and δm_6 :

$$\begin{aligned}
B_6 &= B_6^{\text{UV}} + B_6^{\text{R}} \\
&+ B_{4'} \delta m_2 \\
&+ B_2^{\text{R}} \{2L_4^{\text{UV}} - 4B_2^{\text{UV}} L_{2'}^{\text{UV}} - 7(L_2^{\text{UV}})^2\} \\
&+ B_{2'}^{\text{R}} (B_4^{\text{UV}} - 4B_2^{\text{UV}} L_2^{\text{UV}} - B_2^{\text{UV}} B_{2'}^{\text{UV}}) \\
&- B_{2''}^{\text{R}} (B_2^{\text{UV}})^2 \\
&+ B_{2^{*'}}^{\text{R}} (-2\delta m_2 B_2^{\text{UV}}) \\
&+ \widetilde{B}_4 (4L_2^{\text{UV}}) \\
&+ \widetilde{B}_{4'} (B_2^{\text{UV}}) \\
&+ B_{2^*} (\delta m_4^{\text{UV}} - B_2^{\text{UV}} \delta m_{2'}^{\text{UV}} - 4\delta m_2 L_2^{\text{UV}} - \delta m_2 \delta m_{2^*}^{\text{UV}}) \\
&- B_{2^{**}} (\delta m_2)^2,
\end{aligned} \tag{A25}$$

$$\begin{aligned}
L_6 &= L_6^{\text{UV}} + L_6^{\text{R}} \\
&+ L_{4^*}(\delta m_2) \\
&+ L_2^{\text{R}}\{3L_4^{\text{UV}} - 6B_2^{\text{UV}}L_{2'}^{\text{UV}} - 12(L_2^{\text{UV}})^2\} \\
&+ L_{2'}^{\text{R}}(2B_4^{\text{UV}} - 10B_2^{\text{UV}}L_2^{\text{UV}} - 2B_2^{\text{UV}}B_{2'}^{\text{UV}}) \\
&- L_{2''}^{\text{R}}(B_2^{\text{UV}})^2 \\
&+ \widetilde{L}_4(5L_2^{\text{UV}}) \\
&+ \widetilde{L}_{4'}(B_2^{\text{UV}}) \\
&+ L_{2^*}^{\text{R}}(-2\delta m_2 B_2^{\text{UV}}) \\
&+ L_{2^*}^{\text{R}}(2\delta m_4^{\text{UV}} - 2B_2^{\text{UV}}\delta m_{2'}^{\text{UV}} - 10\delta m_2 L_2^{\text{UV}} - 2\delta m_2 \delta m_{2^*}^{\text{UV}}) \\
&- L_{2^{**}}(\delta m_2)^2, \tag{A26}
\end{aligned}$$

and

$$\begin{aligned}
\delta m_6 &= \delta m_6^{\text{UV}} + \delta m_6^{\text{R}} \\
&- \delta m_{2''}^{\text{R}}(B_2^{\text{UV}})^2 \\
&+ \delta m_{2'}^{\text{R}}(B_4^{\text{UV}} - B_2^{\text{UV}}B_{2'}^{\text{UV}}) \\
&+ \delta m_{2^*}^{\text{R}}(\delta m_4^{\text{UV}} - B_2^{\text{UV}}\delta m_{2'}^{\text{UV}} - \delta m_2 \delta m_{2^*}^{\text{UV}}) \\
&+ \delta m_{2^*}^{\text{R}}(-2\delta m_2 B_2^{\text{UV}}) \\
&+ \delta m_4^{\text{R}}(4L_2^{\text{UV}}) \\
&+ \widetilde{\delta m}_{4^*} \delta m_2 \\
&+ \widetilde{\delta m}_{4'} B_2^{\text{UV}} \\
&- \delta m_{2^{**}}(\delta m_2)^2, \tag{A27}
\end{aligned}$$

where the quantity \widetilde{A} is defined by $\widetilde{A} \equiv A - A^{\text{UV}}$. The difference between \widetilde{A} and A^{R} is that the former contains UV divergent terms arising from subdiagrams, while the latter is completely free from these sub-UV divergences. For instance, we have

$$\begin{aligned}
\widetilde{B}_4 &\equiv B_4 - B_4^{\text{UV}} \\
&= B_4^{\text{R}} + \delta m_2 B_{2^*} + B_2^{\text{UV}}B_{2'}^{\text{R}} + 2L_2^{\text{UV}}B_2^{\text{R}}, \tag{A28}
\end{aligned}$$

$$\begin{aligned}
\widetilde{L}_4 &\equiv L_4 - L_4^{\text{UV}} \\
&= L_4^{\text{R}} + 2\delta m_2 L_{2^*} + 2B_2^{\text{UV}}L_{2'}^{\text{R}} + 2L_2^{\text{UV}}L_2^{\text{R}}, \tag{A29}
\end{aligned}$$

and so on.

We also need the UV divergence structure of M_{4^*} , which is the amplitude of the fourth-order magnetic moment with a two-point vertex insertion:

$$M_{4^*} = M_{4^*}^R + 2L_2^{UV} M_{2^*} + 2(\delta m_2 M_{2^{**}} + B_2^{UV} M_{2^*}) + \delta m_{2^*}^{UV} M_{2^*} . \quad (\text{A30})$$

Substituting the UV structures of the eighth order Eq. (A24), the sixth-order quantities Eqs. (A14), (A25), (A26) and (A27), those of the fourth order Eqs. (A3), (A16), and (A30), and those of the second order (A4) in this sequence in Eq. (A22), we obtain the UV-finite expression of the magnetic moment a_8 :

$$\begin{aligned} a_8 = & M_8^R \\ & + M_6^R(-5B_2^R - 6L_2^R) \\ & + M_4^R\{-4L_4^R - 3B_4^R + 26L_2^R B_2^R + 18(L_2^R)^2 + 9(B_2^R)^2\} \\ & - M_{4^*}^R \delta m_4^R \\ & + M_2\{-B_6^R - 2L_6^R + (B_{2^*} + 4L_{2^*})\delta m_4^R \\ & \quad + 6B_4^R B_2^R + 10B_4^R L_2^R + 12B_2^R L_4^R + 18L_2^R L_4^R \\ & \quad - 30L_2^R (B_2^R)^2 - 54(L_2^R)^2 B_2^R - 30(L_2^R)^3 - 5(B_2^R)^3\} \\ & + M_{2^*}\{-\delta m_6^R + \delta m_4^R(\delta m_{2^*}^R + 6L_2^R + 5B_2^R)\} . \end{aligned} \quad (\text{A31})$$

Again Eq. (A31) has exactly the same structure as Eq. (A22) except that $\delta m_2^R = 0$.

b. I/R-subtraction

In order to handle the numerical calculation on a computer, we need to separate the IR divergent terms from M_8^R . Paying attention to the outermost photon spanning over a self-energy subdiagram, we obtain the IR structure of M_8^R as follows:

$$\begin{aligned} M_8^R = & \Delta M_8 \\ & + M_6^R L_2^R \\ & + M_4^R\{L_4^R - (L_2^R)^2\} \\ & + M_2\{L_6^R - 2L_4^R L_2^R + (L_2^R)^3 - 2\delta m_4^R L_{2^*}^R\} \\ & + M_{4^*}^R \delta m_4^R \\ & + M_{2^*}\{\delta m_6^R - \delta m_4^R \delta m_{2^*}^R - \delta m_4^R L_2^R\} . \end{aligned} \quad (\text{A32})$$

Eq. (A32) has a term $M_{4^*}^R \delta m_4^R$, where $M_{4^*}^R$ is linearly IR-divergent, which arises from the diagrams M_{16} and M_{18} . This term compensates the same IR-divergence found in a_8 of Eq. (A31) whose origin is the mass-renormalization term $M_{4^*} \delta m_4$ associated with the diagrams M_{16} and M_{18} . This IR divergence in M_8^R can thus be removed from M_{16} and M_{18} by the R -subtraction which acts on a fourth-order self-energy subdiagram of M_{16} (M_{18}) and complements the mass-renormalization constant $\delta m_{4a}(\delta m_{4b})$.

Another linear IR divergent term in Eq. (A32) is $2M_2 L_{2^*}^R \delta m_4^R$, where L_{2^*} is linearly divergent. This IR divergence is again found in the diagrams of M_{16} and M_{18} . In the IR-limit of the outermost photon loop, a possible configuration of $M_{16}(M_{18})$ is that the second-order self-energy subdiagram of $M_{16}(M_{18})$ supplies the second-order anomalous magnetic moment M_2 and the fourth-order self-energy subdiagram behaves as $\delta m_{4b(a)}^R$. The IR behavior of the residual diagram including the outermost photon line resembles the second-order vertex diagram with a two-point vertex insertion $L_{2^*}^R$:

$$L_{2^*} \equiv \Delta L_{2^*} + L_{2^*}^R, \quad (\text{A33})$$

where $\Delta L_{2^*} = -3/4$ is the one contraction term of L_{2^*} and the IR divergent $L_{2^*}^R$ is the non-contraction term of L_{2^*} .

This IR divergence in M_8^R of Eq. (A32) compensates the IR divergence in $2M_2 L_{2^*} \delta m_4$ of the renormalized magnetic moment a_8 of Eq. (A31). The origin of the $+4L_{2^*} \delta m_4 M_2$ in Eq. (A31) is the renormalization terms associated with the diagrams M_{08} , M_{10} , M_{41} , and M_{46} . Two of four L_{2^*} terms are exactly canceled by B_{2^*} terms because of the WT-identity $2L_{2^*} + B_{2^*} = 0$. The remaining two L_{2^*} terms will cancel the IR-divergence arising from the diagrams M_{16} and M_{18} in M_8^R .

The last of the linearly IR divergent terms of M_8^R of Eq. (A32) is $M_2 L_6^R$, which also comes from M_{16} and M_{18} . In this case, the second-order self-energy subdiagram supplies a second-order anomalous magnetic moment M_2 and the rest of the residual diagrams are pushed in the IR limit. From $M_{16}(M_{18})$, it gives rise to the similar IR behavior of the six-order vertex renormalization constant $L_{6b(1)}(L_{6c(1)})$. This IR divergence will be canceled in a_8 of Eq. (A31) by the $M_2 L_6^R$ term which comes from the renormalization constants for the diagram $M_{08}(M_{10})$.

To see the cancellation of remaining logarithmic IR divergence in a_8 , we need the IR structures of the renormalization constants L_6^R and B_6^R . Resorting to the WT-identity again,

we can define the finite quantity ΔLB_6 as follows:

$$\begin{aligned}
\Delta LB_6 &\equiv L_6^R + B_6^R \\
&- \{+I_6 + 2L_4^R L_2^R - (L_2^R)^3 + 2\delta m_4^R L_{2^*}\} \\
&- \{-I_6 + L_4^R B_2^R + L_2^R B_4^R - (L_2^R)^2 B_2^R + \delta m_4^R B_{2^*}\}, \tag{A34}
\end{aligned}$$

where I_6 is the overall IR divergent term of L_6 and B_6 . The WT-identity guarantees that ΔLB_6 is independent of the choice of I_6 . Note that $\Delta LB_6 \equiv \Delta L_6 + \Delta B_6 + \Delta L_4 \Delta B_2 + \Delta \delta m_4 B_{2^*}[I]$, where the quantities in the right-hand side are defined in Ref. [32].

c. Finite expression

Separating the UV-finite quantities in a_8 of Eq. (A31) into the IR-singular parts and the finite parts as given in Eqs. (A32), (A18), (A6), (A34), (A20), and (A9), we obtain the expression a_8 in terms of the finite quantities only:

$$\begin{aligned}
a_8 &= \Delta M_8 \\
&+ \Delta M_6(-5\Delta LB_2) \\
&+ \Delta M_4\{-3\Delta LB_4 + 9(\Delta LB_2)^2\} \\
&+ M_2\{-\Delta LB_6 + 6\Delta LB_4 \Delta LB_2 - 5(\Delta LB_2)^3\} \\
&+ 2M_2 \Delta L_{2^*} \Delta \delta m_4. \tag{A35}
\end{aligned}$$

Since $\Delta LB_4 = \Delta L_4 + \Delta B_4$, $2\Delta L_{2^*} = -\Delta B_{2^*}$, and $\Delta LB_2 = \Delta B_2$, this is equivalent to Eq. (76) of Ref. [5], which was obtained from the direct sum of all subtraction terms. Note that the last term of Eq. (A35) remains unsubtracted regardless of the R -subtraction, which is the residual mass-renormalization. This is because we use only the non-contraction term L_2^R as the IR-subtraction term, leaving the finite part of ΔL_{2^*} untouched.

The definition of the finite term ΔL_{2^*} does depend on how to separate IR part from L_{2^*} . To avoid such arbitrariness, we stick to the same I -subtraction rule of IR separation which is used for vertex renormalization constants. Namely, the IR-singularity is confined in L_n^R , which is defined by the rule

$$\begin{aligned}
\widetilde{L}_n &\equiv L_n - \text{highest contraction term of } L_n \\
L_n^R &\equiv \widetilde{L}_n - \text{UV sub-divergence term determined by } K\text{-operation on } \widetilde{L}_n \tag{A36}
\end{aligned}$$

and this L_n^R is used as an IR-subtraction term. This determines $\Delta L_{2^*} = -3/4$ unambiguously. The K -operation does not pick up this ΔL_{2^*} term from a corresponding subdiagram, since L_{2^*} is UV-finite. So, no rule exists in the automation code `GENCODEN` that allows us to subtract the finite term ΔL_{2^*} of a renormalization constant.

The residual renormalization scheme for the Set IV contribution $A_1^{(10)}[\text{Set IV}^{(l_1 l_2)}]$ can be readily obtained from Eq. (A35) by insertion of a closed loop of the lepton l_2 in the internal photon lines of a_8 . This leads to Eq. (17) given in Sec. III.

-
- [1] D. Hanneke, S. Fogwell, and G. Gabrielse, Phys. Rev. Lett. **100**, 120801 (2008).
 - [2] D. Hanneke, S. Fogwell Hoogerheide, and G. Gabrielse, Phys. Rev. A **83**, 052122 (2011).
 - [3] T. Kinoshita and M. Nio, Phys. Rev. D **73**, 053007 (2006).
 - [4] T. Aoyama, M. Hayakawa, T. Kinoshita, and M. Nio, Phys. Rev. Lett. **99**, 110406 (2007).
 - [5] T. Aoyama, M. Hayakawa, T. Kinoshita, and M. Nio, Phys. Rev. D **77**, 053012 (2008).
 - [6] M. Davier, A. Hoecker, B. Malaescu, and Z. Zhang, Eur. Phys. J. **C71**, 1515 (2011).
 - [7] B. Krause, Phys. Lett. **B390**, 392 (1997).
 - [8] K. Hagiwara, R. Liao, A. D. Martin, D. Nomura, and T. Teubner, J. Phys. G **38**, 085003 (2011).
 - [9] K. Melnikov and A. Vainshtein, Phys. Rev. D **70**, 113006 (2004).
 - [10] J. Bijnens and J. Prades, Mod. Phys. Lett. **A22**, 767 (2007).
 - [11] J. Prades, E. de Rafael, and A. Vainshtein, in *Lepton dipole moments*, edited by L. B. Roberts and W. J. Marciano (World Scientific, Singapore, 2009), pp. 303–317.
 - [12] A. Nyffeler, Phys. Rev. D **79**, 073012 (2009).
 - [13] A. Czarnecki, B. Krause, and W. J. Marciano, Phys. Rev. Lett. **76**, 3267 (1996).
 - [14] M. Knecht, S. Peris, M. Perrottet, and E. De Rafael, JHEP **11**, 003 (2002).
 - [15] A. Czarnecki, W. J. Marciano, and A. Vainshtein, Phys. Rev. D **67**, 073006 (2003), **73**, 119901(E) (2006).
 - [16] R. Bouchendira, P. Clade, S. Guellati-Khelifa, F. Nez, and F. Biraben, Phys.Rev.Lett. **106**, 080801 (2011).
 - [17] P. J. Mohr, B. N. Taylor, and D. B. Newell, Rev. Mod. Phys. **80**, 633 (2008).
 - [18] T. Kinoshita and M. Nio, Phys. Rev. D **70**, 113001 (2004).

- [19] T. Aoyama, M. Hayakawa, T. Kinoshita, and M. Nio, Nucl. Phys. **B740**, 138 (2006).
- [20] T. Aoyama, M. Hayakawa, T. Kinoshita, and M. Nio, Nucl. Phys. **B796**, 184 (2008).
- [21] T. Aoyama, M. Hayakawa, T. Kinoshita, M. Nio, and N. Watanabe, Phys. Rev. D **78**, 053005 (2008).
- [22] T. Aoyama, M. Hayakawa, T. Kinoshita, and M. Nio, Phys. Rev. D **78**, 113006 (2008).
- [23] T. Aoyama, K. Asano, M. Hayakawa, T. Kinoshita, M. Nio, and N. Watanabe, Phys. Rev. D **81**, 053009 (2010).
- [24] T. Aoyama, M. Hayakawa, T. Kinoshita, and M. Nio, Phys.Rev.D **82**, 113004 (2010).
- [25] T. Aoyama, M. Hayakawa, T. Kinoshita, and M. Nio, Phys.Rev.D **83**, 053003 (2011).
- [26] T. Aoyama, M. Hayakawa, T. Kinoshita, and M. Nio, Phys.Rev.D **83**, 053002 (2011).
- [27] T. Aoyama, M. Hayakawa, T. Kinoshita, and M. Nio, Phys.Rev.D **84**, 053003 (2011).
- [28] S. Laporta, Phys. Lett. **B328**, 522 (1994).
- [29] J.-P. Aguilar, D. Greynat, and E. De Rafael, Phys.Rev.D **77**, 093010 (2008).
- [30] T. Kinoshita and W. B. Lindquist, Phys. Rev. D **42**, 636 (1990).
- [31] J. A. M. Vermaseren, math-ph/0010025.
- [32] T. Kinoshita, in *Quantum electrodynamics*, edited by T. Kinoshita (World Scientific, Singapore, 1990), pp. 218–321, (Advanced series on directions in high energy physics, 7).
- [33] T. Kinoshita and W. B. Lindquist, Phys. Rev. Lett. **47**, 1573 (1981).
- [34] G. P. Lepage, J. Comput. Phys. **27**, 192 (1978).
- [35] A. Kataev, Phys. Rev. D **74**, 073011 (2006).